Unraveling electronic energy transfer in single conjugated polyelectrolytes encapsulated in lipid vesicles

Pierre Karam[a,b], An Thien Ngo[a,b], Isabelle Rouiller[c], and Gonzalo Cosa[a,b,1]

[a]Department of Chemistry, McGill University, 801 Sherbrooke Street West, Montreal, QC, Canada H3A 2K6; [b]Centre for Self-Assembled Chemical Structures; and [c]Department of Anatomy and Cell Biology, McGill University, Strathcona Anatomy and Dentistry Building, Room 115, 3640 University Street, Montreal, QC, Canada H3A 2B2

Edited by David Whitten, University of New Mexico, Albuquerque, NM, and accepted by the Editorial Board August 13, 2010 (received for review June 8, 2010)

A method for the study of conjugated polyelectrolyte (CPE) photophysics in solution at the single-molecule level is described. Extended observation times of single polymer molecules are enabled by the encapsulation of the CPEs within 200-nm lipid vesicles, which are in turn immobilized on a surface. When combined with a molecular-level visualization of vesicles and CPE via cryo-transmission electron microscopy, these single-molecule spectroscopy studies on CPEs enable us to directly correlate the polymer conformation with its spectroscopic features. These studies are conducted with poly[5-methoxy-2-(3-sulfopropoxy)-1,4-phenylene-vinylene] (MPS-PPV, a negatively charged CPE), when encapsulated in neutral and in negatively charged lipid vesicles. MPS-PPV exists as a freely diffusing polymer when confined in negatively charged vesicles. Individual MPS-PPV molecules adopt a collapsed-chain conformation leading to efficient energy migration over multiple chromophores. Both the presence of stepwise photobleaching in fluorescence intensity-time trajectories and emission from low-energy chromophores along the chain are observed. These results correlate with the amplified sensing potential reported for MPS-PPV in aqueous solution. When confined within neutral vesicles, single MPS-PPV molecules adopt an extended conformation upon insertion in the lipid bilayer. In this case emission arises from multiple chromophores within the isolated polymer chains, leading to an exponential decay of the intensity over time and a broad blue-shifted emission spectrum.

lipid-polymer interaction | exciton migration | water-soluble light-emitting polymer | biosensing

Current knowledge on how the interplay of polymer conformation and chromophore coupling affect energy transfer along a conjugated polymer backbone has been established following rigorous ensemble and single-molecule spectroscopy studies. Many of these studies involve polyphenylene vinylene (PPV)-based conjugated polymers decorated with alkyl side groups that facilitate their solubility in organic solvents. This knowledge is critical for developing conjugated polymer-based electroluminescent, photovoltaic, and sensor devices (1).

The prevailing organization of a polymer backbone is expected to have direct effects on the coupling of neighboring chromophores (planar segments with delocalized π orbitals along the backbone) and on the energy transfer efficiency between these chromophores. Collapsed polymers, predominantly encountered in films prepared from poor solvents, exhibit long-range order where chains are found in close proximity, folded back on themselves (2, 3). Polymers will thus undergo efficient interchain or through-space energy transfer. On the contrary, polymers in solution are highly disordered, where the presence of defects along the chains together with freely accessible bond rotations should result in globular structures with larger intramolecular distances, on average. The predominant mode of energy transfer found in this case is through-bond or intramolecular energy transfer (1, 4–6).

Single-molecule studies conducted on spin-cast conjugated polymers embedded in an inert polymer matrix have highlighted the role played by conformational dependence on conjugated polymer photophysics (2–4, 7–9). Discrete emission levels and on-off single-step transitions characteristic of single chromophores have been observed in the intensity-time trajectories obtained following laser excitation of highly folded single PPV molecules (8). The quantized behavior is due to efficient exciton transport to localized fluorescence quenching defects formed in the PPV backbone (2, 3, 9). In marked contrast, fluorescence intensity-time trajectories from extended PPV chains show an exponential decrease with time, a behavior characteristic of a collection of single chromophores (3). Single-molecule emission spectra are also highly informative. Extended chains are characterized by a broad emission spectrum arising from multiple emission segments with different conjugation lengths (4, 9). Folded chains in turn exhibit emission from a reduced number of low-energy sites with well-defined vibronic structure (3, 4, 9).

These single-molecule studies require the immobilization of PPV polymers in order to prevent their rapid diffusion out of the focal volume of the objective. Monitoring is thus possible for prolonged times. The immobilization is typically achieved by embedding trace amounts of PPV in a polymer matrix such as polymethylmethacrylate (PMMA). This experimental procedure, however, suppresses torsional motions along the polymer backbone and may introduce artifacts arising from the steric hindrance (3, 9, 10).

We report here single-molecule studies on the water-soluble PPV polymer poly[5-methoxy-2-(3-sulfopropoxy)-1,4-phenylene-vinylene] (MPS-PPV, a negatively charged conjugated polyelectrolyte containing the PPV backbone) (11). The limitations of PPV immobilization within a rigid matrix are overcome by encapsulating the polymers within small (*ca.* 200 nm) water-filled lipid vesicles that are in turn anchored on a surface (see Fig. 1). Prolonged observation times are thus achieved while minimizing/suppressing the effect of surface/matrix interactions. Similar strategies have been recently applied to the single-molecule study of activity and conformational fluctuations in proteins (12, 13), ribozymes (14), and protein-DNA interactions (15). This methodology provides an opportunity to examine the photophysics of a conjugated polymer at the single-molecule level for extended periods of time (tens of seconds) while the polymer is fully immersed in solution, devoid of any matrix interactions.

Author contributions: P.K. and G.C. designed research; P.K., A.T.N., and I.R. performed research; P.K., A.T.N., I.R., and G.C. analyzed data; and G.C. wrote the paper.

The authors declare no conflict of interest.

This article is a PNAS Direct Submission. D.W. is a guest editor invited by the Editorial Board.

[1]To whom correspondence should be addressed. E-mail: gonzalo.cosa@mcgill.ca.

This article contains supporting information online at www.pnas.org/lookup/suppl/doi:10.1073/pnas.1008068107/-/DCSupplemental.

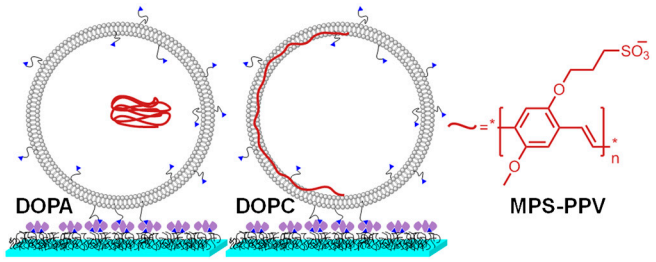

Fig. 1. Cartoon illustrating the encapsulation of MPS-PPV within negatively charged (DOPA:DOPC 3:1) and neutral (DOPC) vesicles. Also illustrated is the vesicle anchoring onto PEG-coated glass coverslips, achieved via biotin-neutravidin interactions (not to scale).

MPS-PPV exists as a freely diffusing polymer when confined in negatively charged vesicles. Individual MPS-PPV molecules adopt a collapsed-chain conformation and display efficient exciton migration. In turn, when confined within neutral (zwitterionic) vesicles, single MPS-PPV molecules readily interact with the vesicle surface and adopt an extended conformation upon insertion in the lipid bilayer. The molecular-level insight gained is critical for developing biosensors based on a liposome beacon concept (16) and more generally toward the utilization of conjugated polyelectrolytes in optoelectronic devices.

Results and Discussion

Ensemble Studies on Conjugated Polyelectrolyte (CPE)-Lipid Vesicle Interactions. We initially searched for conditions that would enable the encapsulation of MPS-PPV within lipid vesicles while minimizing and/or suppressing MPS-PPV binding to the lipid walls, ultimately preserving MPS-PPV freedom of motion within vesicles. Lipid-polymer self-assembly has been observed in mixtures containing surfactants and conjugated polyelectrolytes of opposite charge (17–19) as well as in mixtures of zwitterionic lipids and conjugated polyelectrolytes (16, 20, 21). Experimental conditions involving a lipid mixture of 75% dioleoyl phosphatidic acid (DOPA, an anionic lipid) and 25% dioleoylphosphatidylcholine (DOPC, a zwitterionic lipid) were thus chosen. We reasoned that electrostatic repulsion between the anionic side groups along the polymer backbone and negatively charged lipids should minimize the self-assembly of lipid molecules around the polymer chain.

This hypothesis was tested by monitoring the spectral features of an MPS-PPV solution prior to, and after, addition of preformed lipid vesicles. Addition of an MPS-PPV solution to the 3:1 mole ratio DOPA:DOPC vesicle suspension leads neither to an enhancement nor a blue shift in MPS-PPV emission. Moreover, no extent of Förster resonance energy transfer (FRET) between a membrane-embedded dye DiD (1,1′-dioctadecyl-3,3,3′,3′-tetramethylindodicarbocyanine perchlorate) and MPS-PPV (Fig. 2) is detected. Both an intensity enhancement and a blue shift in intensity, as well as FRET, are observed upon mixing vesicles consisting of 100% DOPC with MPS-PPV. These features are signatures of the association of lipids around the MPS-PPV backbone (16–19). Studies on the encapsulation of MPS-PPV within the 3:1 DOPA:DOPC vesicles and within 100% DOPC vesicles (*SI Appendix*, Fig. S2) further reveal that MPS-PPV interacts with zwitterionic vesicles but not with vesicles consisting of 3:1 DOPA:DOPC. Altogether these results rule out any lipid-polymer interaction in 3:1 DOPA:DOPC vesicles.

Molecular-Level Visualization of Polymer and Vesicles. Encapsulation of MPS-PPV occurs within the 3:1 DOPA:DOPC vesicles upon hydration of dry lipid films with aqueous solutions of MPS-PPV. To compensate for the reduced encapsulation efficiency that anionic lipids might confer, a lyophilization-rehydration step was added to the procedure, prior to extrusion (22, 23). Encapsulation of MPS-PPV was verified via gel filtration chromatography (*SI Appendix*, Figs. S2 and S3) as well as emission quenching of nonencapsulated polymer with membrane-impermeable methyl viologen (16) (*SI Appendix*, Figs. S1 and S4). Under these conditions *ca.* 20% of the total polymer is encapsulated.

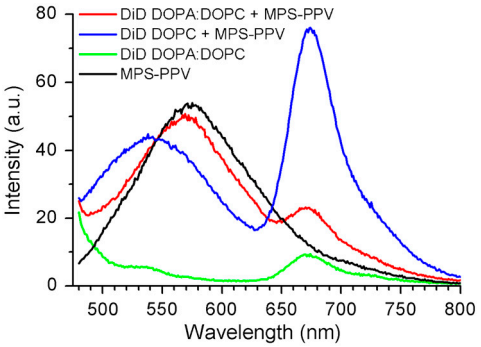

Fig. 2. Emission spectra upon 457-nm excitation of 1.6×10^{-5} M MPS-PPV in monomer units with (red) DOPC vesicles stained with DiD (250:1 lipid:DiD ratio, solutions were 0.20 mM in lipid); (black) DOPA:DOPC (3:1) vesicles stained with DiD (250:1 lipid:DiD ratio, solutions were 0.20 mM in lipid). Also shown is the emission of free MPS-PPV (blue) and of DOPA:DOPC (3:1) vesicles stained with DiD (250:1 lipid:DiD ratio, solutions were 0.20 mM in lipid) (green).

In order to gain an understanding of the polymer and vesicle structures at the molecular level, cryo-transmission electron microscopy (TEM) studies (24, 25) were performed on a series of samples that were 20 mM in lipid and 1.6 mM in polymer monomer units. This is the same polymer/lipid ratio used in the single-molecule spectroscopy studies described below. Vitrified aqueous solutions (16 mM in monomer units of MPS-PPV, no lipids) were also imaged because it was not possible to unequivocally identify polymer particles at lower MPS-PPV concentrations.

Fig. 3*A* is a typical cryoTEM image of free polymer (16 mM in monomer units), where cylindrical, densely packed particles tens of nanometers in length are readily observed. Fig. 3*B* is a representative cryo-TEM image of the 3:1 DOPA:DOPC vesicle sample prepared with MPS-PPV (1.6 mM in monomer units). Five features are apparent: (*i*) There is a large distribution in vesicle size; (*ii*) most vesicles consist of unilamellar lipid bilayers; (*iii*) a few vesicles display bridging between two or three lipid bilayers (yellow arrows); (*iv*) a few vesicles contain a globular cargo appearing as a rippled structure (white arrows); (*v*) the presence of small particles either inside or outside the vesicles are apparent; however, one may not unequivocally assign these as polymer particles or ice contamination.

Control experiments on DOPA:DOPC vesicles with no polymer do not show any major differences compared to the samples described above, indicating a minimal, if any, effect of the polymer on the vesicle morphology. These images indicate that there is little or no interaction between DOPA:DOPC membranes and the polymer. Thus points (*i*) to (*iv*) described above also apply to the controls. Extruded DOPA:DOPC control vesicles are unilamellar and exhibit a large size distribution when imaged via cryoTEM (*SI Appendix*, Fig. S6*C*), as has been previously reported (26). Some extent of bridging between bilayers is also apparent from the previously reported images and the control experiments. Controls also exhibit the globular cargoes described in point (*iv*) above.

Fig. 3*C* shows a representative cryoTEM image of vesicles consisting of 100% DOPC and encapsulating/embedding MPS-PPV. The key features here are the narrower distribution in vesicle size and the prevalence of bridging of multiple lipid bilayers (yellow arrows). MPS-PPV significantly affects the morphology of the DOPC vesicles that otherwise are known to consist of unilamellar

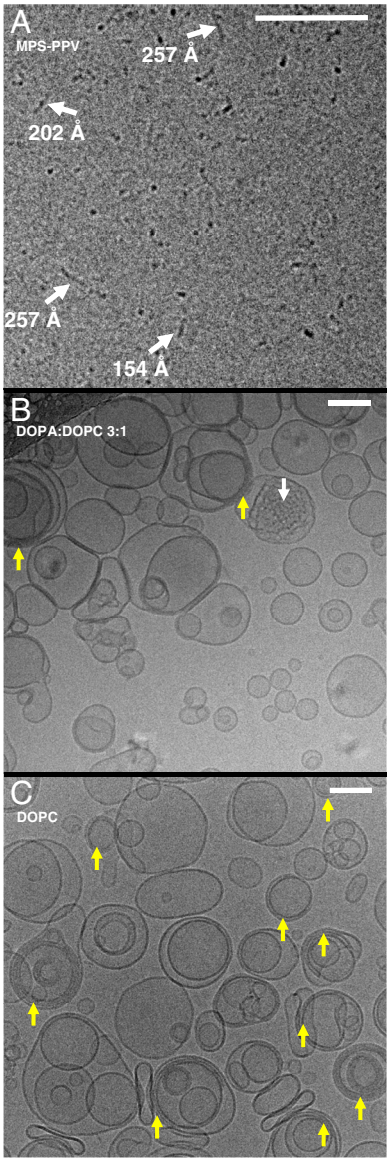

Fig. 3. Cryo-TEM images of (*A*) MPS-PPV with no lipids, the vitrified sample was 16 mM in polymer monomer units. (*B*) DOPA:DOPC 3:1 vesicles. Lipid films were hydrated with an MPS-PPV solution, lyophilized and rehydrated and subsequently extruded through a 200-nm polycarbonate membrane. (*C*) DOPC vesicles. Lipid films were hydrated with an MPS-PPV solution and subsequently extruded through a 200-nm polycarbonate membrane. For images *B* and *C*, the solutions were 20 mM in lipid (*ca.* 50 nM in vesicles) and 1.6 mM in polymer monomer units. The scale bars are 100 nm.

lipid bilayers. The binding of multiple bilayers shown here, mediated by MPS-PPV, presumably arises from MPS-PPV chains that lie intercalated between lipid bilayers. Similar behavior has been reported for other polyelectrolyte-lipid interactions (27).

In an attempt to unequivocally observe both MPS-PPV particles and vesicles, the polymer concentration was increased 10-fold, to 16 mM, while keeping constant the lipid concentration at 20 mM. These conditions accentuated the DOPC lipid-polymer interactions observed in Fig. 3*C* leading to densely packed vesicles (*SI Appendix*, Figure S6*D*). Interestingly, for the 3:1 DOPA:DOPC preparations, upon increasing the MPS-PPV concentration both vesicles and the formation of ordered structures are observed (*SI Appendix*, Fig. S6 *A* and *B*). We note that these conditions represent a 2,000% increase in polymer monomer:lipid molecular ratio. These conditions may very well represent a previously undescribed sector in the morphological phase diagram for lipid-MPS-PPV aggregates.

To conclude this section, the cryo-TEM results together with the ensemble spectroscopy results shown in Figs. 2 and 3 and *SI Appendix* confirm that MPS-PPV is encapsulated, yet freely moving, within negatively charged (3:1 DOPA:DOPC) vesicles. Additional verification on the encapsulation is provided by the fluorescence imaging studies described below. These studies also show that MPS-PPV is adsorbed to the zwitterionic (100% DOPC) lipid membranes, possibly intercalated within the lipid bilayers where it adopts an extended conformation and facilitates the binding of multiple bilayers. By tuning the lipid charge in the vesicles, one can ultimately obtain vesicles with a freely diffusing MPS-PPV in a folded conformation over vesicles with a membrane bound MPS-PPV in an extended conformation.

The different vesicles described provide a unique vehicle in which to study the emission intensity and emission spectra characterizing single MPS-PPV molecules in various conformations in aqueous solutions over extended periods of time, as described below.

Surface-Anchored Vesicles Encapsulating MPS-PPV. The next goal was to ensure that the vesicles (both neutral and negatively charged) contain either one or no MPS-PPV molecules. Whereas single fluorescent dyes can be pinpointed on the basis of their narrow single-molecule intensity distribution and their single-step photobleaching, neither property is extendable to single-molecule studies on single emissive conjugated polymers. First, the large polydispersity inherent to the synthesis of conjugated polymers leads to a large distribution in their emission intensity. Second, the sample preparation method has an effect on whether the polymer will behave as a single quantum state (displaying single-step photobleaching) or as a collection of independent chromophores.

Our approach to determining the encapsulation number involves assessing the number of occupied vesicles over the total number of vesicles anchored to the surface under study. The estimated probability of vesicles containing one, two, or more MPS-PPV molecules can thus be calculated. In order to count the total number of vesicles, the lipophilic probe DiD was incorporated at a 1:20,000 DiD:lipid mole ratio, effectively achieving a load of 20 DiD fluorophores per 200-nm diameter vesicle. The fluorophore DiD serves as a positional marker of the entire vesicle. It can be selectively excited at 633 nm and its emission recorded without contamination from MPS-PPV emission (16).

The vesicles for single-molecule studies were prepared by supplementing lipid mixtures with biotin-tagged lipids in order to anchor the vesicles onto the surfaces via biotin-streptavidin interactions (see Fig. 1). The vesicle preparations were first diluted and subsequently immobilized on glass coverslips previously coated with a biotin-PEG:PEG mixture and to which neutravidin was added. The coating prevents vesicle rupture and ensures specific vesicle anchoring (see Fig. 1) (14–16).

Single particle fluorescence images were obtained with a raster-scan confocal fluorescence microscope. The emission was collected with a high numerical aperture objective and split into two channels via a 640-nm dichroic mirror. Whereas DiD emission was detected only in the red channel [control experiments with vesicles containing up to 40 DiD molecules per liposome in the absence of MPS-PPV showed no emission in the green channel consistent with the onset of DiD emission being at 640 nm], MPS-PPV was principally detected in the green channel with some leakage into the red channel. The images show diffraction-limited spots (*ca.* 300 nm in diameter) resulting from the emission of the encapsulated MPS-PPV polymer upon 514 nm excitation (Fig. 4 *A* and *B*) or the membrane-embedded DiD emission when exciting at 633 nm (Fig. 4*C*).

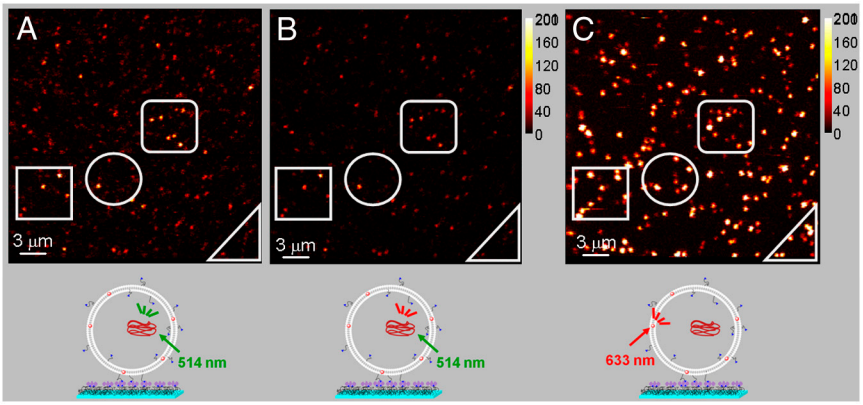

Fig. 4. Fluorescence scanning confocal images for MPS-PPV encapsulated in anionic vesicles (DOPA : DOPC; 3 : 1) containing *ca.* 20 DiD/vesicle. The vesicles were prepared as described in the caption of Fig. 3 and further separated from free polymer via gel filtration chromatography and diluted to a final 100-pM concentration prior to surface immobilization. *A* (green channel) and *B* (red channel) were acquired simultaneously upon 514-nm excitation of MPS-PPV. *C* was obtained upon directly exciting vesicle embedded DiD with the 633-nm line of a HeNe laser. The right bar illustrates the counts per millisecond per pixel.

Images of DOPA : DOPC 3 : 1 vesicles prepared upon hydration with MPS-PPV solutions are shown in Fig. 4 *A–C*. Colocalization is observed between MPS-PPV (514-nm excitation) and 3 : 1 DOPA : DOPC vesicles (633-nm excitation) providing additional evidence that MPS-PPV is encapsulated inside the vesicles. A total of 46 vesicles containing MPS-PPV were recorded upon exciting at 514 nm by selecting a 40 counts/ms threshold. With 633-nm excitation, 265 vesicles were recorded. The number of empty vesicles, *ca.* 83% of the total, greatly outnumbers those encapsulating MPS-PPV. This is visually confirmed in the images shown in Fig. 4 *A* and *C*. The probability that a vesicle encapsulates more than a single MPS-PPV molecule is therefore negligible under the experimental conditions used here.

Preparations of DOPC vesicles and MPS-PPV were also imaged. Given the high affinity of MPS-PPV for the zwitterionic lipids and in order to ensure that most vesicles contain either one or no polymer, the neutral vesicles were prepared with a low MPS-PPV monomer : lipid ratio, 25-fold smaller than that used for 3 : 1 DOPA : DOPC. Only 24% of the vesicles are observed to be interacting with MPS-PPV under these conditions, ensuring that most vesicles contain only one MPS-PPV molecule.

Single-Molecule Emission Intensity and Spectra. The effective immobilization of vesicles encapsulating MPS-PPV enables the study of the polymer photophysics in solution at the single-molecule level, and for extended periods of time. Experiments consisted of both intensity vs. time trajectories, acquired upon excitation at 514 nm, and of single-molecule emission spectra recorded on an electron-multiplied, back-illuminated CCD camera using 488-nm excitation. The studies were conducted on single MPS-PPV molecules when encapsulated in 3 : 1 DOPA : DOPC and when embedded in DOPC. No DiD was included in these preparations.

Fig. 5*A* shows a representative intensity vs. time trajectory for a single MPS-PPV polymer molecule in 3 : 1 DOPA : DOPC, acquired upon excitation at 514 nm. Close inspection reveals the presence of stepwise photobleaching akin to that observed in previous studies for collapsed forms of MPS-PPV embedded in polymer films (3, 9). The transients display discrete on-off (reversible) transitions as well as transitions to intermediate intensity states in *ca.* 66% of the molecules (Figs. 5*A* and 6*A*, *Inset*). In the remaining 34% of the molecules a gradual intensity decrease with time is observed upon continued excitation. In some cases (22% of the total), small steps were observed, but the dominant decay is exponential in nature. Although care was

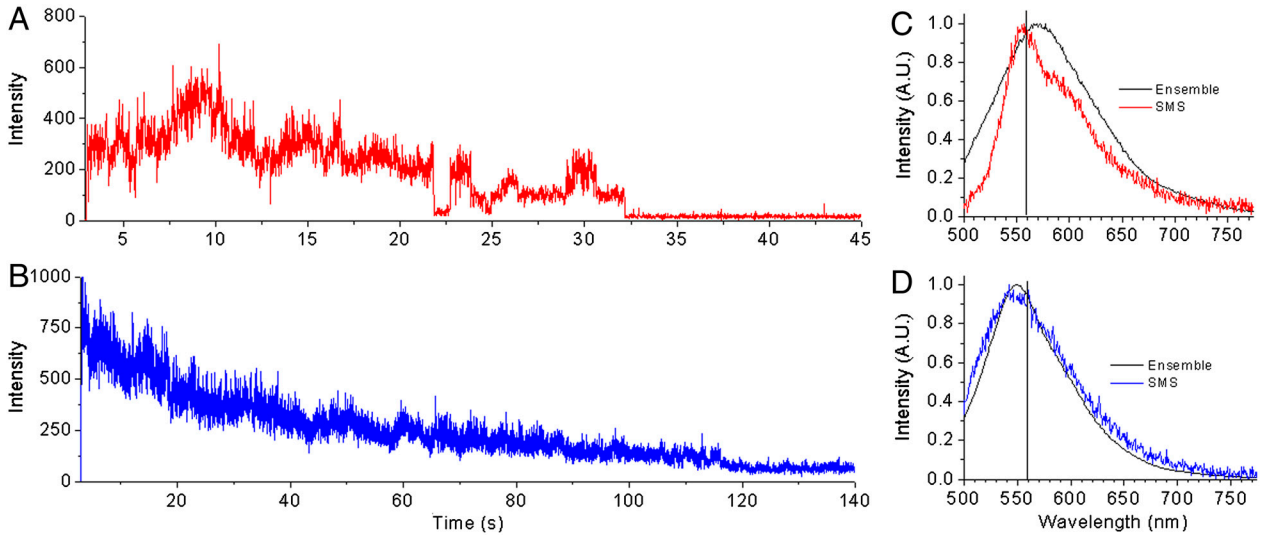

Fig. 5. Intensity-time trajectories acquired upon 514-nm excitation of MPS-PPV encapsulated in vesicles containing no DiD (10-ms dwell time). (*A*) Anionic vesicles (DOPA : DOPC; 3 : 1) and (*B*) neutral vesicles (DOPC). *C* and *D* show single-molecule emission spectra (labeled SMS for single molecule spectra) for MPS-PPV in (*C*) anionic vesicles (DOPA : DOPC; 3 : 1) and (*D*) neutral vesicles (DOPC) obtained upon 488-nm excitation and using a 500-nm long pass filter. Overlaid (black traces, labeled Ensemble) are ensemble steady-state emission spectra acquired for the same samples.

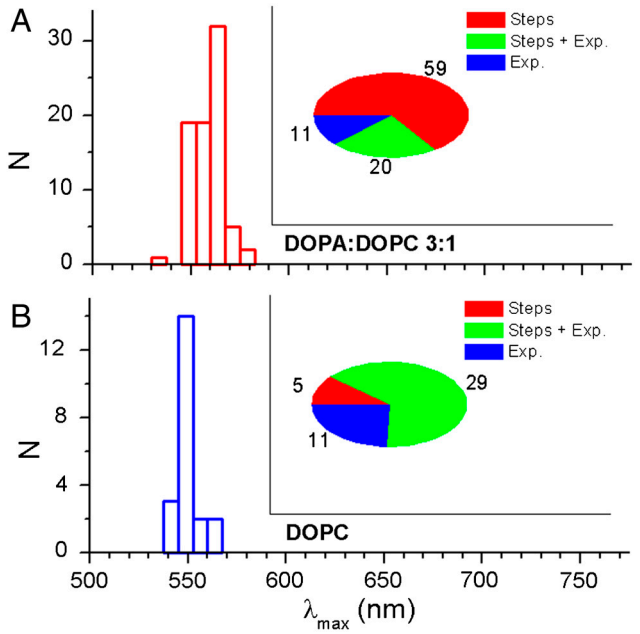

Fig. 6. Distribution of the peak wavelength (λ_{max}) for the emission spectra of single MPS-PPV molecules when encapsulated in DOPA:DOPC 3:1 (*A*) or in DOPC (*B*). The inset pie plots portray the total number of molecules with discrete on-off (reversible) transitions as well as transitions to intermediate intensity states (red, steps), and the number of molecules that follow a gradual intensity decrease with time upon continued excitation (exponential and steps plus exponential).

taken to remove oxygen from the solutions via the combined action of glucose/glucose-oxidase and catalase, the large extent of reversible photobleaching is likely due to trace O_2 in solution. This would also account for the relatively short survival time of the fluorescent molecules. Fluorescence intensity time trajectories only a few tens of seconds in duration are obtained before irreversible photobleaching occurs.

Spectra of MPS-PPV molecules encapsulated in 3:1 DOPA:DOPC typically exhibit maxima at 558 nm (see Fig. 5*C*). Most of the 78 molecules monitored under these conditions show vibronic structure (Fig. 5*C*). In addition to the 0-0 band at 558 nm a shoulder at *ca.* 595 nm was observed. This is *ca.* 0.14 eV below the first vibronic peak and corresponds to the backbone stretching mode, a vibronic pattern typical of π-π* transitions in PPV polymers (2, 3). The emission from the remaining molecules in 3:1 DOPA:DOPC, albeit peaked at 558 nm, showed a rather broad emission extending in the blue region and lacking vibronic structure. It is remarkable that we observe a vibronic pattern for the freely diffusing polymer encapsulated within anionic vesicles. This pattern indicates that the spectra arise from a few emissive sites (chromophores) within the polymer backbone and that energy is efficiently funneled to these sites (2, 3). This is counterintuitive for a polymer that is readily exploring its conformational space over time, where conjugated segments are affected by torsional motions that would give rise to a broad continuous distribution. The polymer likely remains coiled in water favoring rapid energy migration to a few low-energy sites (560 nm, *ca.* 2.2 eV).

It is interesting to compare the results for MPS-PPV in 3:1 DOPA:DOPC with those obtained for the closely related conjugated polymer poly[2-methoxy-5-(2'ethyl-hexyloxy)1,4-phenylene-vinylene] (MEH-PPV) when immobilized in films at room temperature (3, 9) and at 20 K (10). Fluorescence spectra for single MEH-PPV molecules recorded at room temperature have a bimodal distribution in peaks with maxima at 560 nm and 580 nm, characteristic of two different types of conformations being trapped in the polymer matrix. In contrast the MPS-PPV emission peak distribution is centered around a single peak at 560 nm (a single molecule was recorded with the 580-nm emission pattern). The 580-nm component in MEH-PPV arises from exciton interactions upon chain–chain contacts in parallel oriented chromophores. It is not surprising that this species is not observed because chain–chain contacts would demand a high electrostatic penalty in the polyanionic MPS-PPV. The emission spectra of MEH-PPV spin-cast from toluene, a poor solvent, have a well-defined vibronic structure in a PMMA host matrix at room temperature (3, 9), highly accentuated at 20 K (10). The less defined vibronic structure observed for freely diffusing MPS-PPV at room temperature is consistent with the polymer being in a fluid media solvated by water.

In closing the description of spectral properties of MPS-PPV in 3:1 DOPA:DOPC, we note that under the experimental conditions used here, a significant extent of reversible photobleaching (see above) is observed in addition to a spectral blue shift in the polymer emission upon continuous irradiation. This is consistent with O_2-mediated destruction of low-energy chromophores (*SI Appendix*, Fig. S7).

The single-molecule results obtained in 3:1 DOPA:DOPC show that MPS-PPV single molecules adopt a collapsed-chain conformation, leading to efficient energy migration over multiple chromophore units. However, the results obtained in neutral vesicles are markedly different. Fig. 5*B* shows a representative intensity vs. time trajectory for a single MPS-PPV polymer molecule in DOPC. An exponential decrease in emission intensity with time is observed for *ca.* 90% of the molecules studied under these conditions (Fig. 6*B*). MPS-PPV encapsulated in DOPC vesicles exhibited a broad emission with no apparent vibronic pattern and centered at *ca.* 545 nm, 15 nm to the blue in comparison to results in anionic vesicles (Figs. 5*D* and 6*B*). These results are consistent with MPS-PPV molecules adopting an extended conformation upon insertion in the lipid bilayer, with poor exciton migration overall. The emission of single MPS-PPV molecules in DOPC likely results from the broad distribution of quasilocalized chromophores on the polymer chain. Notably, there is little difference between ensemble and single-molecule spectra for MPS-PPV in DOPC (Fig. 5*B*), in line with the argument that the MPS-PPV polymer molecule consists of a large number of independent chromophores when embedded in DOPC and in stark contrast to results in the 3:1 DOPA:DOPC system (see above).

Conclusions

By carefully tuning the lipid composition, lipid vesicles entrapping freely diffusing conjugated polyelectrolyte MPS-PPV have been prepared, as have vesicles with membrane bound MPS-PPV. The different vesicles provide a means to study the emission intensity and emission spectra characterizing single MPS-PPV molecules in various conformations in aqueous solutions over extended periods of time. The molecular-level visualization of vesicles and MPS-PPV via cryo-TEM, together with single-molecule spectroscopy results on MPS-PPV, enable one to directly correlate the polymer conformation with its spectroscopic features. MPS-PPV in aqueous solution adopts a collapsed-chain conformation leading to efficient energy migration over multiple chromophore units. These results correlate with the amplified sensing potential reported for MPS-PPV in aqueous solution. When confined within neutral vesicles, single MPS-PPV molecules are shown to adopt an extended conformation upon insertion in the lipid bilayer, characterized by poor energy migration.

Materials and Methods

Lipid Vesicle Preparation. Dry lipid films were prepared from chloroform solutions. The solvent was evaporated by a stream of argon, and the resulting thin lipid film was placed under vacuum for at least 30 min to remove the remaining solvent. In order to encapsulate MPS-PPV (Sigma-Aldrich) within vesicles, dry lipid films were hydrated with a pH 7.3 solution 1.6 mM in MPS-PPV monomer units, 150 mM in NaCl, and 10 mM in Hepes. The final

lipid concentration was 20 mM. The samples were subjected to 10 freeze-thaw-sonication cycles (vesicles prepared from 3:1 mole ratio DOPA:DOPC required an additional lyophilizing and rehydration step). DOPC vesicles were then extruded through a 200-nm polycarbonate membrane. The extruded samples were filtered through a column of Sephacryl 500 HR. The vesicle size was characterized with a dynamic light scattering system. Further details are included in *SI Appendix*.

Cryo-TEM Studies. Five microliters of vesicle solution or MPS-PPV solution were added to glow-discharged QUANTIFOIL® R 2/2. Samples were blotted and frozen hydrated by plunging into a bath of liquid ethane slush (25, 28). They were stored under liquid nitrogen temperature until transfer to a 626 Single Tilt Cryotransfer System (Gatan Inc.) and observed with a FEI G2 F20 cryo-STEM microscope operated at 200 KV (FEI, Inc). Further details are included in *SI Appendix*.

Single-Molecule Studies. Glass coverslips were functionalized with a mixture of PEG and biotin PEG (Laysan Bio, Inc.) in order to prevent vesicle rupture and nonspecific adsorption of vesicles or free MPS-PPV (14–16). Following neutravidin incubation vesicles containing 1% biotin DPPE were immobilized on PEG-coated glass coverslips via biotin-neutravidin interactions (14–16). Flow chambers (10 μL) were prepared with a predrilled polycarbonate film (GraceBio) with an adhesive gasket that was assembled on top of the PEG-treated surface. Silicone ports were glued on top of the chamber. In order to increase polymer photostability, all experiments were run under a constant flow of an oxygen scavenger solution consisting of β-mercaptoethanol 1% vol/vol, β-D(+)glucose 3% wt/vol, glucose oxidase 0.1 mg/mL, and catalase 0.02 mg/mL. Solutions were pH 7.3, 10 mM in Hepes buffer, and 150 mM in NaCl. All experiments were conducted at room temperature (22–23 °C). Details on the experimental setup are included in *SI Appendix*.

ACKNOWLEDGMENTS. G.C. and I.R. are grateful to Natural Sciences and Engineering Research Council and Canadian Foundation for Innovation New Opportunities Fund for financial assistance. P.K. and A.T.N. are also thankful to the McGill Chemical Biology Fellowship Program (Canadian Institutes of Health Research) for postgraduate scholarships.

1. Scholes GD, Rumbles G (2006) Excitons in nanoscale systems. *Nat Mater* 5:683–696.
2. Hu DH, et al. (2000) Collapse of stiff conjugated polymers with chemical defects into ordered, cylindrical conformations. *Nature* 405:1030–1033.
3. Huser T, Yan M, Rothberg LJ (2000) Single chain spectroscopy of conformational dependence of conjugated polymer photophysics. *Proc Natl Acad Sci USA* 97:11187–11191.
4. Schwartz BJ (2003) Conjugated polymers as molecular materials: How chain conformation and film morphology influence energy transfer and interchain interactions. *Annu Rev Phys Chem* 54:141–172.
5. Collini E, Scholes GD (2009) Coherent intrachain energy migration in a conjugated polymer at room temperature. *Science* 323:369–373.
6. Beljonne D, et al. (2002) Interchain vs intrachain energy transfer in acceptor-capped conjugated polymers. *Proc Natl Acad Sci USA* 99:10982–10987.
7. Schindler F, Lupton JM, Feldmann J, Scherf U (2004) A universal picture of chromophores in π-conjugated polymers derived from single-molecule spectroscopy. *Proc Natl Acad Sci USA* 101:14695–14700.
8. VandenBout DA, et al. (1997) Discrete intensity jumps and intramolecular electronic energy transfer in the spectroscopy of single conjugated polymer molecules. *Science* 277:1074–1077.
9. Yu J, Hu DH, Barbara PF (2000) Unmasking electronic energy transfer of conjugated polymers by suppression of O-2 quenching. *Science* 289:1327–1330.
10. Lee YJ, Kim DY, John KG, Paul FB (2005) Variable temperature single-molecule dynamics of MEH-PPV13. *ChemPhysChem* 6:2404–2409.
11. Chen L, et al. (1999) Highly sensitive biological and chemical sensors based on reversible fluorescence quenching in a conjugated polymer. *Proc Natl Acad Sci USA* 96:12287–12292.
12. Rhoades E, Cohen M, Schuler B, Haran G (2004) Two-state folding observed in individual protein molecules. *J Am Chem Soc* 126:14686–14687.
13. Boukobza E, Sonnenfeld A, Haran G (2001) Immobilization in surface-tethered lipid vesicles as a new tool for single biomolecule spectroscopy. *J Phys Chem B* 105:12165–12170.
14. Okumus B, Wilson TJ, Lilley DMJ, Ha T (2004) Vesicle encapsulation studies reveal that single molecule ribozyme heterogeneities are intrinsic. *Biophys J* 87:2798–2806.
15. Cisse I, Okumus B, Joo C, Ha T (2007) Fueling protein-DNA interactions inside porous nanocontainers. *Proc Natl Acad Sci USA* 104:12646–12650.
16. Ngo AT, Karam P, Fuller E, Burger M, Cosa G (2008) Liposome encapsulation of conjugated polyelectrolytes: Toward a liposome beacon. *J Am Chem Soc* 130:457–459.
17. Dalvi-Malhotra J, Chen L (2005) Enhanced conjugated polymer fluorescence quenching by dipyridinium-based quenchers in the presence of surfactant. *J Phys Chem B* 109:3873–3878.
18. Chen L, Xu S, McBranch D, Whitten D (2000) Tuning the properties of conjugated polyelectrolytes through surfactant complexation. *J Am Chem Soc* 122:9302–9303.
19. Treger JS, et al. (2008) Tuning the optical properties of a water-soluble cationic poly (p-phenylenevinylene): Surfactant complexation with a conjugated polyelectrolyte. *J Phys Chem B* 112:760–763.
20. Ding L, et al. (2009) Insight into the mechanism of antimicrobial poly(phenylene ethynylene) polyelectrolytes: Interactions with phosphatidylglycerol lipid membranes. *Langmuir* 25:13742–13751.
21. Ngo AT, Cosa G (2010) Assembly of zwitterionic phospholipid/conjugated polyelectrolyte complexes: Structure and photophysical properties. *Langmuir* 26:6746–6754.
22. Torchilin VP, Weissig V, eds. (2003) *Liposomes* (Oxford Univ Press, New York).
23. Gregoriadis G, Saffie R, Hart SL (1996) High yield incorporation of plasmid DNA within liposomes: Effect on DNA integrity and transfection efficiency. *J Drug Target* 3:469–475.
24. Frederik PM, Hubert DHW, Nejat D (2005) *Methods Enzymol* (Academic, New York), pp 431–448.
25. Almgren M, Edwards K, Karlsson G (2000) Cryo transmission electron microscopy of liposomes and related structures. *Colloid Surface A* 174:3–21.
26. Traïkia M, Warschawski DE, Lambert O, Rigaud J-L, Devaux PF (2002) Asymmetrical membranes and surface tension. *Biophys J* 83:1443–1454.
27. Luan Y, Ramos L (2007) Real-time observation of polyelectrolyte-induced binding of charged bilayers. *J Am Chem Soc* 129:14619–14624.
28. Dubochet J, et al. (1988) Cryo-electron microscopy of vitrified specimens. *Q Rev Biophys* 21:129–228.